Acta Oceanol. Sin., 2014, Vol. 33, No. 7, P. 97–106
DOI: 10.1007/s13131-014-0509-3
http://www.hyxb.org.cn
E-mail: hyxbe@263.net

On the surface roughness characteristics of the land fast sea-ice in the Bohai Sea

LIU Chengyu[1,2], CHAO Jinlong[1,3], GU Wei[1]*, LI Lantao[1,3], XU Yingjun[1]

[1] State Key Laboratory of Earth Surface Processes and Resource Ecology, Beijing Normal University, Beijing 100875, China
[2] Shanghai Institute of Technical Physics, Chinese Academy of Sciences, Shanghai 200083, China
[3] Academy of Ministry of Civil Affairs and Ministry of Education for Disaster Reduction and Emergency Management, Beijing Normal University, Beijing 100875, China

Received 16 July 2012; accepted 19 February 2014

Abstract

The surface roughness characteristics (e.g., height and slope) of sea ice are critical for determining the parameters of an electromagnetic scattering, a surface emission and a surface drag coefficients. It is also important in identifying various ice types, retrieval ice thickness, surface temperature and drag coefficients from remote sensing data. The point clouds (a set of points which are usually defined by *X*, *Y*, and *Z* coordinates that represents the external surface of an object on earth) of land fast ice in five in situ sites in the eastern coast Bohai Sea were measured using a laser scanner-Trimble GX during 2011–2012 winter season. Two hundred and fifty profiles selected from the point clouds of different samples have been used to calculate the height root mean square, height skewness, height kurtosis, slope root mean square, slope skewness and slope kurtosis of them. The root mean square of the height, the root mean square of the slope and the correlation length are about 0.090, 0.075 and 11.74 m, respectively. The heights of 150 profiles in three sites manifest the Gaussian distribution and the slopes of total 250 profiles distributed exponentially. In addition, the fractal dimension and power spectral density profiles were calculated. The results show that the fractal dimension of land fast ice in the Bohai Sea is about 1.132. The power spectral densities of 250 profiles can be expressed through an exponential autocorrelation function.

Key words: sea ice, roughness, statistical parameters, fractal dimension, spectral density

Citation: Liu Chengyu, Chao Jinlong, Gu Wei, Li Lantao, Xu Yingjun. 2014. On the surface roughness characteristics of the land fast sea-ice in the Bohai Sea. Acta Oceanologica Sinica, 33(7): 97–106, doi: 10.1007/s13131-014-0509-3

1 Introduction

Sea ice has caused a lot of adverse impacts on an offshore aquaculture, a marine transportation, and an offshore oil engineering. To limit these adverse impacts, it is critical to collect the information of sea ice (thickness, extent and concentration) precisely. A remote sensing technology has superiority for obtaining real-time and large-scale sea ice information, and it has played an important role in sea ice monitoring in the Bohai Sea in recent years.

As a general rule, the sea-ice surface is always rough (Wadhams, 2000). So most of the sea-ice surface in the Bohai Sea are also not smooth, but rough and uneven (Ding, 1999). The roughness of the sea-ice surface can influence the distribution characteristics of a sea-ice reflectance, the scattering coefficient and emissivity in different directions and the average value of these parameters in 2π space corresponding to the space above the sea-ice surface whose solid angle is just 2π (Xu, 2006; Jin, 1993), which may generate errors in the inversion of sea-ice thickness and surface temperature using remote sensing data.

Previous studies on the roughness of sea ice were focused on the sea ice near the Arctic Ocean and Antarctic waters. Using airborne laser altimeter measurements, Mai et al. (1996) determined the distance and the size of the floating ice in the Fram Strait using the frequency distribution characteristics of the height of the sea-ice surface above water and estimated the drag coefficient of the sea-ice surface using these results. Hibler III and Leschack (1972) obtained the contour data from the underside and surface of the sea-ice in the Arctic Ocean using a sonar and a laser scanner based on an energy spectrum analysis. The results show that the distribution of the ice ridge is not random on the bottom of the sea-ice; there is great difference between multiyear sea-ice and one-year sea-ice. Rivas et al.(2006) obtained the surface contour of the sea-ice in Veaufort, Chukchi and the Bering Sea using an airborne lidar technology, and calculated the power spectral density function, correlation length and root mean square of the born ice, one-year flat ice, one-year non-flat ice and multiyear ice in the three sea areas. The results show that the Lorentz function describes the power spectral density function of the height of the sea-ice surface in these sea areas fairly well. Dierking (1995) obtained the height data of the sea-ice surface in the Weddell Sea based on a laser altimeter, analysed the relation between the height of sea-ice ridges and their distances and showed an exponential relationship between them. Using a fractal analysis, Gneiting et

Foundation item: The National High Technology Research and Development Program of China under contract No. 2011AA100505 ; the National Key Technology R&D Program of China under contract No. 2006BAB03A03; the State Key Laboratory of Earth Surface Processes and Resource Ecology, Beijing Normal University of China under contract Nos 2010-TD-02 and 2011-TDZD-050.
*Corresponding author, E-mail: weigu@bnu.edu.cn

al. (2010) has calculated the fractal dimension of the parabola of the arctic sea-ice surface. In contrast, studies on the roughness features of the sea ice in the Bohai Sea are relatively rare. Li et al. (2009) monitored the fixed sea ice near the Liaodong Gulf with CCD cameras, using the probability distribution features of the height of hummocked ice and the cutting angle of the profile. We are not aware of any detailed surface roughness characteristics investigation.

In recent years, Trimble GX 3D laser scanner has been widely used in the research of microgeomorphology. It can conveniently obtain the morphology data of a ground surface with a standard derivation of 6.5 mm at a distance of 200 m, so it is feasible to apply such an instrument to the in situ study of the sea-ice surface roughness.

The statistical parameters, the fractal dimension and the power spectral densities are common parameters used to describe the roughness of sea ice. The statistical parameters include the mean, root mean square, skewness, kurtosis and frequency histogram. The calculation of the statistical parameters is quicker for the sea- ice surface height data because it can rapidly consider the status of the sea-ice surface height distribution. However, it is difficult to fit and simulate the surface morphology of the sea ice. The fractal dimension can reflect the roughness of the surface profile (Davies and Hall, 1999; Gneiting and Schlather, 2004). Within the known fractal dimension, we can simulate the rough surface according to certain functions of fractal characteristics and calculate other related parameters (Jaggard and Sun, 1990; Franceschetti et al., 1996). For example, according to the fractal dimension, the rough surface can be simulated well with Weierstrass-Mandelbrot function (Guo et al., 2010). To a certain extent, the power spectral density can eliminate the apparatus and sampling errors that are inevitable in an actual measurement. In addition, it is easier to establish the relationship between the surface statistics and the surface reflectivity through the power spectral density (Stover, 1995).

In order to provide the qualitative and quantitative features of the Bohai Sea ice surface roughness, which can later be used for better estimate the ice type, the ice thickness and the surface temperature drag coefficients from the remote sensing data, we measured the point clouds in five in situ sites in the eastern coast Bohai Sea using a laser scanner-Trimble GX during 2011 to 2012 winter season and 250 profiles were selected to calculate the statistical parameters (height root mean square (rms), height skewness, height kurtosis, slope root mean square, slope skewness and slope kurtosis), the power spectral density and their fractal dimensions, under the assumption that the roughness of the sea-ice surface is isotropic. Concrete qualitative and quantitative information of surface roughness characteristics of land fast ice in the Bohai Sea were obtained after summarizing the calculated results.

2 Field measurement

2.1 *Instrument*

A Trimble GX 3D laser scanner made by Trimble Navigation Company (USA) was used. The main wavelength of the laser pulse is 532 nm, with a field range of 360°×60°, a scan resolution of 3 mm at a distance of 50 m, a standard deviation of 6.5 mm at a distance of 200 m, a horizontal scanning range of 200 000 points and a vertical one of 65 536 points. The instrument uses an automatic level compensation and a real-time temperature compensation. It also can run an atmospheric correction resulting in point cloud output, a set of points which are usually defined by *X*, *Y*, and *Z* coordinates, and represents the external surface of an object on the earth.

2.2 *Locations and programs*

Field measurements were made in January and February 2012, during a period where the maximum amount of sea-ice formed in the Bohai Sea in the winter of 2011 to 2012. The overall ice condition of the winter of 2011 to 2012 was a normal ice year in the Bohai Sea (NCSBSOAPRC, 2013). The maximal thickness of the single layer level ice of the Liaodong Gulf, the Bohai Gulf and the Laizhou Gulf was 45, 20 and 20 cm, respectively, and the common thickness was 10–20, 5–10 and 10–20 cm, respectively (NCSBSOAPRC, 2013). The maximal distance of the sea-ice edge from the coasts of the Liaodong Gulf, Bohai Gulf and Laizhou Gulf was 74, 24 and 23 km, respectively, and the maximal sea-ice area of Liaodong Gulf, Bohai Gulf and Laizhou Gulf was 21 001, 6 346 and 3 306 km^2 (NCSBSOAPRC, 2013).

Five sites in the eastern coast Bohai Sea were selected for the field measurements (Fig. 1). The concrete sea-ice condition and meteorological measurements were listed in Table 1. The

Table 1. The sea ice and weather conditions *in situ*

	Sample 1	Sample 2	Sample 3	Sample 4	Sample 5
Date	2012-02-05	2012-01-15	2012-02-15	2012-02-09	2012-01-13
Description	melting and freezing on the surface	collision and small ice pieces	collision and large ice pieces	violent collision	stranded ice, stranded on the reef
Measured sea- ice thickness/cm	35–38	30–38	30–40	25–45	30–42
Sea ice concentration within 0.5 km from the coast/%	about 95	about 95	about 90	about 90	about 95
Snow cover	no	no	no	no	no
Air temperature/°C	–1.55	–2.82	–4.45	–2.02	–2.16
Wind speed/m·s^{-1}	3.713	2.257	1.587	2.221	1.093
Measured area/m^2	800	36 000	39 000	39 000	20 000
Resolution	4 mm @ 10 m	4 mm @ 10 m	6 mm @ 10 m	4 mm @ 10 m	5 mm @ 10 m

Notes: The numerical orders from Sample 1 to Sample 5 were on the basis of ice ages. "4 mm @ 10 m" means the resolution is 4 mm at a distance of 10 m.

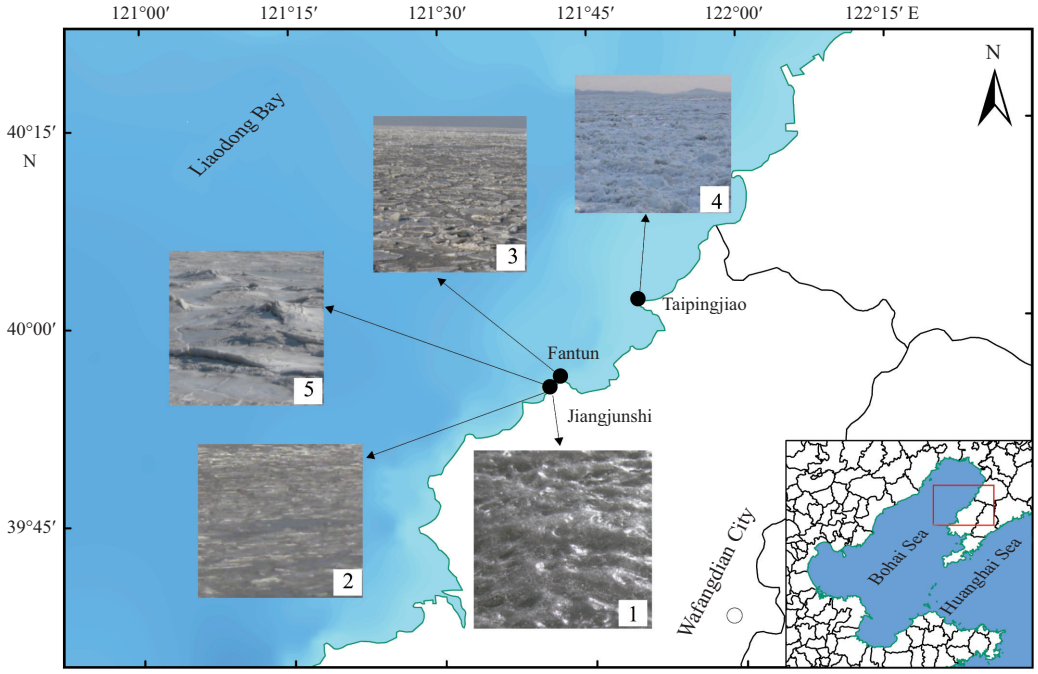

Fig.1. The spatial distribution of the sea-ice measurement locations. The photo numbers denote the sample numbers.

weathers were fine during our measurements, and the temperatures were below 0 °C, so the ice samples were not melting. The rougher the surface was, the larger the measured area was. Considering the time-consuming nature of the measurement and the spatial resolution, the scan resolution was set to be 4–6 mm at a distance of 10 m during the measurement (Table 1).

3 Results and analysis

As a general rule, the point cloud obtained by the Trimble GX 3D laser scanner was the point cloud on one side of the sea ice. We assumed that the roughness characteristics of the sea ice are isotropic. Fifty profiles were selected from the point cloud of each sample listed in Table 1 (a total of 250 lines). The total height distribution histogram, root mean square (σ_z) of height, height skewness (α_z), height kurtosis (κ_z), correlation length (l_z), the slope (s) distribution histogram, the mean slope ($\overline{s}$), root mean square (σ_s) of the slope, height skewness (α_s), and slope kurtosis (κ_s), the fractal dimension and the power spectral density of each sample were calculated. The methodology of data processing is presented in the Appendix.

3.1 *The characteristics of the statistical parameters*

In general, rough sea ice is primarily formed by the freezing and thawing effect on the smooth ice surface (Sample 1) or refreezing of ice pieces (Samples 2–5). Figure 2 shows the height and slope versus frequency histograms of samples. The number of bins in each histogram was 30, and the slope was represented by the tangent value. On the basis of Fig. 2 and Table 2, it is clear that Sample 1 which formed mainly by freezing and thawing, has rms of only 0.009 m. The mean slope of Sample 1 is the smallest (0.013), and the rms of the slope is 0.015. Sample 2 is a single-layer sea ice that formed from the ice pieces and its surface height is higher than that of Sample 1, with a height rms of 0.027 m, a mean slope of 0.019 and a slope rms of 0.019. The forming processes of Samples 2 and 3 were basically same, while the size of the ice pieces was different (Sample 3 being larger than Sample 2, with a height rms of 0.061, a mean slope is of 0.065, and a slope rms of 0.093). Sample 4 was formed as a

Table 2. The statistical parameters and fractal dimensions of the various sample section lines

	Nd/m	σ_z/m	α_z	κ_z	$\overline{s}$	σ_s	α_s	κ_s	l_z/m	$\overline{D}_2$
Sample 1	13.0	0.009	-1.052	2.826	0.013	0.015	1.741	3.397	2.4	1.087
Sample 2	120.0	0.027	0.335	2.493	0.019	0.019	3.299	38.595	20.0	1.134
Sample 3	150.0	0.061	1.554	7.396	0.065	0.093	2.877	13.539	8.7	1.154
Sample 4	203.8	0.218	0.257	3.188	0.190	0.281	2.806	12.505	15.6	1.169
Sample 5	79.8	0.136	0.661	3.894	0.087	0.120	3.979	23.710	12.0	1.118

Notes: Nd is the length of the selected profile with N sampling points and a resolution of d, and the detail information is in Appendix.

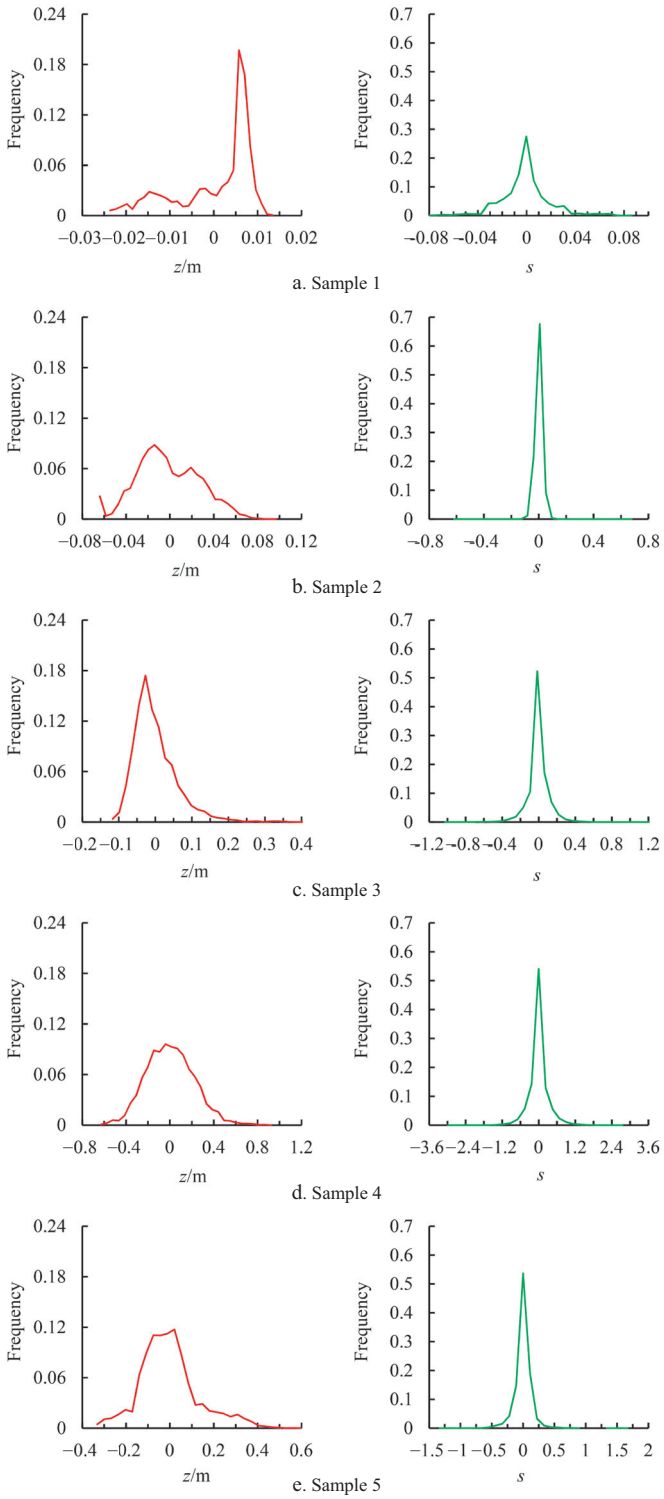

Fig.2. The height (z) frequency and slope versus frequency histograms of the various samples. The left column is the height frequency histograms and the right column is the slope frequency histograms. The slope is calculated from Eq. (2b)

result of a severe collision, and its ice pieces cannot be clearly observed. For Sample 4, the height of the rms (0.218 m) increased significantly, the mean slope is 0.190 and the rms slope is 0.281. Sample 5 formed as the sea ice floated to the shore at high tide and was stranded or at low tide. Sample 5 has a height rms of 0.136 m, a mean slope of 0.087 and an rms slope of 0.120. Regarding the height skewness with third-order statistics, the height frequency histograms are skewed to the right except

Table 3. A chi-square test of the height versus frequency histograms and slope versus frequency histograms

	Sample 1	Sample 2	Sample 3	Sample 4	Sample 5
Normal distribution	36.35	4.60	10 803.95	0.88	4.80
Threshold (*Prob*=0.95)	16.93	16.93	16.93	16.93	16.93
Exponential distribution	2.91	11.50	12.39	12.95	15.52
Threshold (*Prob*=0.95)	17.71	17.71	17.71	17.71	17.71

for Sample 1, which has a skewness of –1.052 and is therefore skewed to the left. For the height kurtosis of fourth-order statistics, the kurtosis of Samples 1 and 2 are lower than those of the normal distribution (3.0), and the kurtosis of the other three samples are greater than the normal distribution. In regards to skewness and kurtosis of the slope, Sample 2 has the maximal kurtosis of 38.595, but the kurtosis of Sample 1 is only 2.652. The order of the degree of kurtosis is Sample 2 greater than Sample 5 greater than Sample 3 greater than Sample 4 greater than Sample 1. We found that the slope skewness is the only statistical parameter for which stranded ice (Sample 5) is greater than all other ice types.

Table 3 is a comparison table that illustrates the chi-square test score values of the height versus frequency histogram and slope versus frequency histogram. The height versus frequency histogram was based on the assumption of the normal distribution and is expressed as

$$f(z)=\frac{1}{\sqrt{2\pi}\sigma_z}\exp\left[-\frac{(z-\overline{z})^2}{2\sigma_z^2}\right], \tag{1}$$

where $f(z)$ represents the probability density function; $\overline{z}$ is an average value; σ_z is the root mean square. The slope versus frequency histogram was based on the assumption of exponential distribution and was expressed as

$$f(s')=\frac{1}{2\overline{s}}\exp\left(-|s'|/\overline{s}\right), \tag{2a}$$

$$s'_{\mathrm{r},p,n}=\frac{z_{\mathrm{r},p,n+1}-z_{\mathrm{r},p,n}}{x_{\mathrm{r},p,n+1}-x_{\mathrm{r},p,n}}, \tag{2b}$$

where $f(s')$ is the probability density function; $s'_{\mathrm{r},p,n}$ is the slope of profile p with sample n that considers the aspect, and the negative values indicate that their aspects are π; $z_{\mathrm{r},p,n}$ is the relative height. The formula of the chi-square test (Bendat and Piersol, 2010) is

$$\chi^2=\sum_{i=1}^{M}\frac{O_i-E_i}{E_i}M, \tag{3}$$

where χ^2 is a chi-square value; O_i is a measured value; E_i is a theoretical value; M represents the number of samples. On the basis of Table 3, the height versus frequency histograms of Samples 1 and 3 do not fit the normal distribution, while Samples 2, 4 and 5 are normally distributed. The slopes of all five samples are distributed exponentially and only the chi-square value of Sample 5 is close to the threshold.

3.2 *Fractal dimension characteristics*

Table 4 shows that the fractal dimensions of five samples are greater than their geometric dimensions (1.0). The maximum fractal dimension was observed for Sample 4 (1.169), while the minimum is for Sample 1 (1.087). The maximum of the fractal dimension is less than 1.2, which is also less than the fractal dimension in the arctic sea-ice (approximately 1.38) (Gneiting et al., 2010). This shows that the roughness of the one-year sea-ice in the Bohai Sea is not much larger than the multiyear sea ice. Table 4 shows the correlation coefficient between the statistical parameters presented in Table 2. The height of the rms (σ_z) is correlated significantly with the mean slope ($\overline{s}$) and the slope of rms (σ_s) (the correlation coefficient is 0.98 and 0.97, respectively). The mean slope ($\overline{s}$) was closely related to that slope of rms (σ_s), while the kurtosis (α_s) of the slope was related to the relative length (l_z). This may have occurred because there was a certain similarity in the calculation method of these statistics. In addition, the second-order statistics have a low correlation with third-order and fourth-order statistics. For example, the correlation coefficient between height of

Table 4. The correlation coefficient between different parameters

	σ_z/m	α_z	κ_z	$\overline{s}$	σ_s	α_s	κ_s	l_z/m	$\overline{\hat{D}}_2$
σ_z/m	1.00	0.25	-0.03	0.98	0.97	0.38	-0.09	0.36	0.63
α_z		1.00	0.78	0.26	0.25	0.63	0.34	0.36	0.68
κ_z			1.00	0.05	0.06	0.10	-0.24	-0.28	0.38
$\overline{s}$				1.00	1.00	0.22	-0.20	0.31	0.72
σ_s					1.00	0.20	-0.22	0.29	0.72
α_s						1.00	0.73	0.64	0.32
κ_s							1.00	0.84	0.18
l_z/m								1.00	0.59
$\overline{\hat{D}}_2$									1.00

rms (σ_z) and height of kurtosis (α_z) is only –0.03. The highest correlation occurred between the fractal dimension ($\hat{D}_2$) and the mean slope ($\bar{s}$) and the fractal dimension ($\hat{D}_2$) and the slope of rms (σ_s); both are 0.72. In practical applications, to reduce the redundancy of the information, we can select only one parameter for analysis with high correlation statistics.

3.3 *The characteristics of power spectral density*

The figures from Fig. 3a to e show that the profiles of the surface height and power spectral density of Sample 1 to Sample 5. The left column of Fig. 3 is the profiles of the surface height, and the right column is the profiles of the power spectral density. The minimums of spatial frequency of the five samples are not identical because of the different sampling intervals. The values are 0.0769, 0.0083, 0.0067, 0.0049 and 0.0125 m^{-1}, for Samples 1–5, respectively. The maximum value is the same for all samples with a value of 5 m^{-1}. The sequence of the power spectral density values of the five samples is as follows: Sample 4>Sample 5>Sample 3>Sample 2>Sample 1. This order corresponds to the order of the root mean square of the height in Table 2. For the purpose of analysing the characteristics of the power spectral density of the height profiles, the hypothesis is that the autocorrelation functions of height profiles may be expressed by a Gaussian autocorrelation function and an exponential autocorrelation function, and the Chi-square test is also carried out based on Eq. (3).

The formula of the Gaussian autocorrelation function is

$$g(r)=\delta_z^2\exp(\frac{-r^2}{l_z}), \tag{4}$$

where $g(r)$ represents the autocorrelation function, $r=x_2-x_1$, is the distance in the x direction. The power spectral density of the Gaussian autocorrelation function is expressed as

$$d_{\mathrm{ps,G}}(f)=\frac{\delta_z^2 l_z}{2\sqrt{\pi}}\exp\left(\frac{-f^2 l_z^2}{4}\right), \tag{5}$$

where $d_{\mathrm{ps,G}}(f)$ represents the power spectral density of Gaussian auto-correlation function; f is the frequency. The expression of the exponential auto-correlation function is:

$$g(r)=\delta_z^2\exp(\frac{-|r|}{l_z}). \tag{6}$$

The power spectral density is

$$d_{\mathrm{ps,G}}(f)=\frac{\delta_z^2 l_z}{\pi(1+f^2 l_z^2)}. \tag{7}$$

In Eqs (5) and (7), the power spectral density function is only related to the height of rms (σ^2) and correlation length (l_z). The height of rms (σ^2) and correlation length (l_z) can be substituted in Table 2 into the Eqs (5) and (7), respectively, to calculate the chi-square (χ^2) value using Eq. (3) and the power spectral density ($d_{\mathrm{ps,G}}(f)$) in Fig. 3. The results are shown in Table 4.

In Table 5, the power spectral density of the five samples is closer to the power spectral density of the exponential autocorrelation function (i.e., the height autocorrelation function is the exponential autocorrelation function). Moreover, in Fig. 3 the spatial frequency is less than 1.0 m^{-1}, when the calculated values of the power spectral density and the power spectral density exponential autocorrelation function are closer, and with the increase of frequency, the difference between the two increased. This may be caused by errors that occurred during measurement and the resample process.

4 Discussion and conclusions

Five in situ sites in the eastern coast Bohai Sea were selected, and the land fast ice surface heights were measured using the Trimble GX 3D laser scanner in January and February 2012, during the period with the maximum sea-ice formation in the Bohai Sea in the winter of 2011 to 2012. The statistical parameters, fractal dimension and power spectral density of the 250 profiles selected from the sea-ice surface height data were calculated, and the following primary conclusions were drawn. First, the heights of 150 profiles in three sites show the Gaussian distribution and the slopes of total 250 profiles show the exponential distribution. The root mean square of height, root mean square of slope and the correlation length of land fast ice in the Bohai Sea are about 0.090, 0.075 and 11.74 m, respectively. Second, the fractal dimensions are larger than the corresponding geometric dimensions for all the samples, and the fractal dimension is about 1.132. Thirdly, the power spectral densities of total 250 profiles are the exponential autocorrelation function. The errors in this study are mainly caused by the laser scanner and the data resampling.

The statistical parameters, the fractal dimension and the power spectral density are related to the resolution and quantity of the samples, which are referred to the scale effect. The statistical parameters, the fractal dimension and the power spectral density may be different for different samples on different scales. The ratio of the wavelength to the surface height must be considered to calculate the electromagnetic energy from the scattering and the emission. To estimate the quantity of the electromagnetic energy from the scattering and emission more accurately for sea ice, we must investigate the characteristics of roughness of sea ice on different scales. As described in Section 3, there is a relationship among the statistical parameters, especially the root mean square of height and the root mean square of slope, fractal dimension and the power spectral density. This may be attributed to the sea-ice surface roughness or the methods of calculation.

In general, the statistical parameters are used to measure the sea-ice surface roughness when establishing the empirical

Table 5. The power spectral density and chi-square test

	Sample 1	Sample 2	Sample 3	Sample 4	Sample 5
Exponential autocorrelation function	0.07	84.96	234.99	563.24	92.90
Gaussian autocorrelation function	126 771	4.72×10^{22}	6.78×10^{30}	1.41×10^{20}	1.33×10^{107}
Threshold (*Prob*=0.95)	64.94	598.71	748.85	1 018.06	398.50

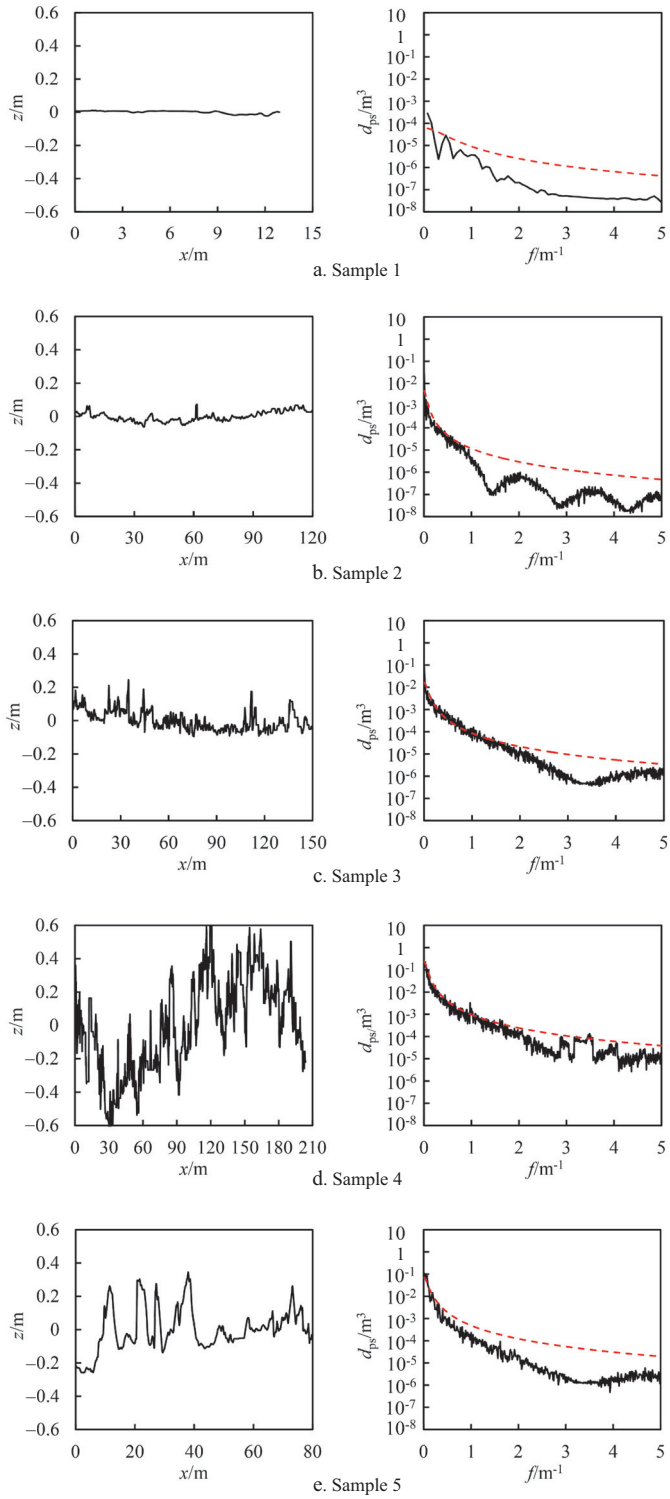

Fig.3. The height profile and power spectral density ($d_{p,s}$) curve of different samples. The left column represents the height curve and the right column represents the power spectral density curve. The black solid line is the practical calculation value of the power spectral density and the red dotted line is a theoretical calculations of the power spectral density for the exponential distribution.

models. However, the fractal dimension and the power spectral density are used more frequently to represent the sea ice surface roughness if the semi empirical models or mathematical and physical models are constructed. Understanding the roughness characteristics of the sea-ice surface is important for improving the accuracy of determining the thickness of the sea-

ice, the temperature of sea-ice surface, and the drag coefficients using remote sensing data. For the sea-ice thickness inversion, if one knows the parameters (root mean square of height, root mean square of slope, and different models need different inputs) describing the characteristics of the surface roughness, the amount of surface scattering can be calculated using surface scattering approximation methods (Kirchhoff approximation, small perturbation method) (Jin, 1993), then it can be put into a sea-ice radiation transfer equation to determine the sea-ice thickness combined with the related structural parameters (porosity, contents of brine pockets and bubbles, particle size distributions of brine pockets and bubbles, spatial distributions of brine pockets and bubbles). When the scatter is reflection symmetric, the value depends on the surface roughness and on the local incidence angle. There is a sensitive decrease of circular polarization coherence with increasing of the product of the wavenumber and the rms of the height in the microwave band, over a range of 0 to 1, because of the depolarizing effects of small-scale surface slopes (Mattia et al., 1997; Schuler et al., 2002). And the relationship is mainly exponential in C-band (Gupta et al., 2013). For the inversion of the sea-ice surface temperature, the thermal infrared radiation of the sea-ice surface can be modelled with the parameters of the sea-ice surface roughness (Hapke, 1993; Li et al., 1993; Liu et al., 2013), and the accuracy of temperature estimation of the sea-ice surface can be improved by means of calculating the sea-ice emissivity at different viewing angles with different rms of height in the Bohai Sea via the so-called linear kernel driver model (Liu, 2013). For the drag coefficient inversion, one can conveniently estimate the drag coefficient of the sea-ice surface after inputting the parameters of the sea-ice surface roughness (for example, root mean square of height) into the formulas for the estimation of the drag coefficients (Banke and Smith, 1973; Mai et al., 1996; Steiner et al., 1999).

In this paper, we provide the quantitative description on the sea ice surface roughness in the Bohai Sea, which may further be applied to sea-ice modelling. Our future work will be focused on the quantitative description of roughness of float ice to compare the different characteristics of surface roughness of land fast ice and float ice to give an overall description of surface roughness of all ice types in the Bohai Sea.

References

Banke E G, Smith D S. 1973. Wind stress on Arctic sea ice. Journal of Geophysical Research, 78(33): 7871–7883

Bendat J S, Piersol A G. 2010. Random Data Analysis and Measurement Procedures. Hoboken: John Wiley & Sons, 79–108

Davies S, Hall P. 1999. Fractal analysis of surface roughness by using spatial data. Journal of the Royal Statistical Society Series, B61: 3–37

Dierking W. 1995. Laser profiling of the ice surface topography during the winter Weddell gyre study. Journal of Geophysical Research, 100(C3): 4807–4820

Ding Dewen. 1999. Introduction of Sea Ice Engineering (in Chinese). Beijing: China Ocean Press, 1–70

Franceschetti G, Migliaccio M, Riccio D. 1996. An electromagnetic fractal-based model for the study of fading. Radio Science, 31(6): 1749–1759

Gneiting T, Schlather M. 2004. Stochastic models that separate fractal dimension and the Hursteect. SIAM Review, 46: 269–282

Gneiting T, Ševčíková H, Percival D B. 2010. Estimators of fractal dimension: assessing the roughness of time series and spatial data, Technical Report No.577. Washington: University of Washington, 1–33

Guo Lixin, Wang Rui, Wu Zhensen. 2010. Basic Theory and Methods of Randomly Rough Surface Scattering. Beijing: Science Press, 1–30

Gupta M, Scharien R K, Barber D G. 2013. C-band polarimetric coherences and ratios for discriminating sea ice roughness. International Journal of Oceanography, 1–13

Hapke B. 1993. Theory of Reflectance and Emittance Spectroscopy. Combridge: Combridge University Press, 358–385

Hibler III W D, Leschack L A. 1972. Power spectrum analysis of undersea and surface sea-ice profiles. Journal of Glaciology, 11: 345–356

Jaggard D L, Sun X. 1990. Scattering from fractally corrugated surfaces. Journal of the Optical Society of America, 7(6): 1131–1139

Jin Yaqiu. 1993. Electromagnetic Scattering and Thermal Radiation Theory of Remote Sensing (in Chinese). Beijing: China Science Press, 194–210

Li Xiaowen, Strahler A H, Zhu Qijiang, et al. 1993. Bidirectional reflection of rough surface composed of basic units–Mutual shielding geometric-optical model. Chinese Science Bulletin, 38(1): 86–89

Li Zhijun, Kong Xiangpeng, Zang Yong, et al. 2009. Field investigations of piled ice forming in coastal area. Journal of Dalian Maritime University (in Chinese), 35(3): 9–12

Liu Chengyu. 2013. A study on characteristics of surface roughness, multi angular optical reflection and thermal infrared emission of sea ice in the Bohai Sea based on in situ measurements [dissertation]. Beijing: Beijing Normal University, 79–85

Liu Chengyu, Gu Wei, Li Lantao, et al. 2013. Study on the impact of surface roughness on the directional characteristic of infrared radiation of sea ice in the Bohai Sea. Marine Forecasts, 30(4): 1–11

Mai S, Wamser C, Kottmeier C. 1996. Geometric and aerodynamic roughness of sea ice. Boundary-Layer Meteorology, 77: 233–248

Mandelbrot B B. 1982. The Fractal Geometry of Nature. New York: Freeman, 25–108

Mattia F, Toan T L, Souyris J, et al. 1997. The effect of surface roughness on multifrequency polarimetric SAR data. IEEE Transactions on Geoscience and Remote Sensing, 35(4): 954–966

NCSBSOAPRC. 2013. Communique of Maritime Hazard of North China Sea in 2012 (in Chinese). Qingdao: North China Sea Branch of State Oceanic Administration, People's Republic of China, 15–20

Rivas M B, Maslanik J A, Sonntag J G, et al. 2006. Sea ice roughness from airborne LIDAR profiles. IEEE Transactions on Geoscience and Remote Sensing, 44(11): 3032–3037

Schuler D L, Lee J, Kasilingam D, et al. 2002. Surface roughness and slope measurements using

polarimetric SAR data. IEEE Transactions on Geoscience and Remote Sensing, 40(3): 687–698

Steiner N, Harder M, Lemke P. 1999. Sea-ice roughness and drag coefficients in a dynamic–thermodynamic sea-ice model for the Arctic. Tellus, 51A: 964–978

Stover J C. 1995. Optical Scattering Measurement and Analysis. Bellingham: SPIE Optical Engineering Press, 45–50

Wadhams P. 2000. Ice in the ocean. Amsterdam: Gordon and Breach Science Publishers, 1–73

Xu Xiru. 2006. Physical Theory of Remote Sensing (in Chinese). Beijing: Perking University Press, 20–245

Appendix. Data processing

The selected profiles were resampled with a resolution of 0.1 m. Subtracting the mean of the profile, the resulting line was denoted by $(x_{p,n}, z_{r,p,n})$, p is the serial number of the profile, and n is the serial number of the sampling points, $n \in \{0,1,2,3,\cdots,N-1\}$, where N is the amount of the sampling points. $x_{p,n}$ is the abscissa of the sample (which was the profile p with the sample n), and $z_{r,p,n}$ is the relative height of profile p of Sample n.

1 Statistic parameters

The total height distribution histogram, root mean square (σ_z) of height, height skewness (α_z), height kurtosis (κ_z), correlation length (l_z), the slope (s) distribution histogram, the mean slope ($\bar{s}$), root mean square (σ_s) of the slope, height skewness (α_s), and slope kurtosis (κ_s) of the 50 profiles of each sample were calculated. The formulas used to calculate statistical parameters were listed in Table A1.

2 Fractal dimension

The fractal analysis has been widely applied in a data analysis involving time, section line and surface profiles in almost all disciplines (Mandelbrot, 1982). The main methods used to calculate the fractal dimension are the box-count method, the Hall-Wood method, the variation method, the energy conversion method, the semiperiodogram method, and the wavelet transform method. Gneiting et al. (2010) have shown that the variation method is more suitable for the fractal analysis of spatial data, so we chose this method to calculate the fractal dimension of the sea-ice surface section line. One-dimensional discrete data $z_{r,p,n}$ was calculated as previously described:

$$\hat{D}_{p,q} = 2 - \frac{\left\{\sum_{l=1}^{L}(s_l - \bar{s})\ln\left[\hat{V}_{p,q}(l/N)\right]\right\}}{q\sum_{l=1}^{L}(s_l - \bar{s})}, \tag{A1}$$

$$V_{p,q}(l/N) = \frac{1}{2(N-l)}\sum_{n=l}^{N-1}\left|z_{r,p,n} - z_{r,p,n-l}\right|^q, \tag{A2}$$

where q represents the time of the variation; q generally takes a value of 1/2, 1 or 2; $\hat{D}_{p,q}$ represents the fractal dimension when the time was q; s_l=ln(l/N), represents the logarithm value of the measurement scale; $\bar{s}$ represents the average of the s_l; $\hat{V}_{p,q}(l/N)$ represents the energy change value when q was the time and l/N was measurement scale; and L represents the series of the measurement scale, $L \geqslant 2$. It is better for spatial data when L and q were assigned the number 2 according to the Gneiting et al. (2010) studies.

In the actual calculation of the fractal dimension, the procedure was as follows: first, calculate the fractal dimensions $\hat{D}_{p,2}$ for each section line of all samples using Eqs (1) and (2); and second, set the average value of all the fractal dimensions of section lines $\bar{\hat{D}}_2$ as the selected sample's surface height fractal dimension. Set N to 100 when calculating each fractal

Table A1. Formulas used to calculate statistical parameters

Parameter	Formula
$z_{r,p,n}$	$z_{p,n} - \frac{1}{N}\sum_{n=0}^{N-1}\bar{z}_{p,n}$
σ_z	$\frac{1}{PN}\sum_{p=0}^{P-1}\sum_{n=0}^{N-1}z_{r,p,n}^2$, $P=50$
α_z	$\frac{1}{P}\sum_{p=0}^{P-1}\frac{1}{\sigma_{z,p}^3}\sum_{n=0}^{N-1}z_{r,p,n}^3$, $\sigma_{z,p} = \frac{1}{N}\sum_{n=0}^{N-1}z_{r,p,n}^2$
κ_z	$\frac{1}{P}\sum_{p=0}^{P-1}\frac{1}{\sigma_{z,p}^4}\sum_{n=0}^{N-1}z_{r,p,n}^4$
l_z	$\rho_{z,p}(l) = \frac{\sum_{n=0}^{N-l}z_{r,p,n}z_{r,p,n+l}}{\sigma_{z,p}^2}$, $\rho(l_{z,p}) = \frac{1}{e}$, $l_z = \frac{1}{P}\sum_{p=0}^{P-1}l_{z,p}$
$\bar{s}$	$\frac{1}{PN}\sum_{p=0}^{P-1}\sum_{n=0}^{N-1}s_{r,p,n}$, $s_{r,p,n} = \left\lvert\frac{z_{r,p,n+1} - z_{r,p,n}}{x_{r,p,n+1} - x_{r,p,n}}\right\rvert$
σ_s	$\frac{1}{PN}\sum_{p=0}^{P-1}\sum_{n=0}^{N-1}\left(s_{r,p,n} - \bar{s}_{r,p}\right)^2$, $\bar{s}_{r,p} = \frac{1}{N}\sum_{n=0}^{N-1}s_{r,p,n}$
α_s	$\frac{1}{P}\sum_{p=0}^{P-1}\frac{1}{\sigma_{s,p}^3}\sum_{n=0}^{N-1}(s_{r,p,n} - \bar{s}_{r,p})^3$, $\sigma_{s,p} = \frac{1}{N}\sum_{n=0}^{N-1}\left(s_{r,p,n} - \bar{s}_{r,p}\right)^2$
κ_s	$\frac{1}{P}\sum_{p=0}^{P-1}\frac{1}{\sigma_{s,p}^4}\sum_{n=0}^{N-1}(s_{r,p,n} - \bar{s}_{r,p})^4$

dimension of profiles, and then move forward in increments of 5. Calculate the fractal dimension of each slide. Then consider the mean of the fractal dimensions calculated using the sliding method to be the fractal dimension of the profile.

3 Power spectral density

The power spectral density of the discrete data $(x_{p,n}, z_{\tau,p,n})$ with the number N was calculated as:

$$d_{ps}(f_k) = \hat{d}_{ps}(f_k) = \frac{1}{P}\sum_{p=1}^{P}\frac{d}{N}\left|\sum_{n=1}^{N-1} e^{-\left(\frac{j2\pi kn}{N}\right)} z_{\tau,p,n}\right|^2, \quad \text{(A3)}$$

where P represents the amount of the section line for sampling; $z_{\tau,p,n}$ represents the profile p; d represents the sampling interval; $x_{p,n} = nd$, $0 \leqslant x_{p,n} \leqslant (N-1)d$; and $f_k = \frac{k}{Nd}$, $\frac{1}{Nd} \leqslant f_k \leqslant \frac{1}{2d}$. The interval of the frequency is $\Delta f = \frac{1}{Nd}$. So k ranges from 1 to $N/2$ according to Nyquist theorem.